Bone 128 (2019) 115036

Contents lists available at ScienceDirect

Bone

journal homepage: www.elsevier.com/locate/bone

Full Length Article

Novel ActRIIB ligand trap increases muscle mass and improves bone geometry in a mouse model of severe osteogenesis imperfecta

Josephine T. Tauer[a,c], Frank Rauch[b,c,*]

[a] Faculty of Dentistry, McGill University, Montreal, Quebec, Canada
[b] Department of Pediatrics, McGill University, Montreal, Quebec, Canada
[c] Shriners Hospital for Children-Canada, Montreal, Quebec, Canada

ARTICLE INFO

Keywords:
ACE-2494
Activin
Animal model
Bone
Muscle
Osteogenesis imperfecta

ABSTRACT

Osteogenesis imperfecta (OI) caused by mutations affecting the extracellular matrix protein collagen type I is characterized by fragile bones and low muscle mass and function. Activin A and myostatin, members of the TGF-β superfamily, play a key role in the control of muscle mass and in muscle-bone communication. Here we investigated activin A/myostatin signaling in a mouse model of severe dominant OI, *Col1a1*$^{Jrt/+}$mouse, and the effect of activin A/myostatin inhibition by a soluble activin receptor IIB receptor, ACE-2494, on bones and muscles in 8-week old mice. Compared to wild type mice, *Col1a1*$^{Jrt/+}$mice had elevated TGF-β signaling in bone and muscle tissue. ACE-2494 treatment of wild type mice resulted in significantly increased muscle mass, bone length, bone mass as well as improved bone mechanical properties. However, treatment of *Col1a1*$^{Jrt/+}$mice with ACE-2494 was associated with significant gain in muscle mass, significantly improved bone length and bone geometry, but no significant treatment effect was found on bone mass or bone mechanical properties. Thus, our data indicate that activin A/myostatin neutralizing antibody ACE-2494 is effective in stimulating muscle mass, bone length and diaphyseal bone growth but does not correct bone mass phenotype in a mouse model ofdominant OI.

1. Introduction

Osteogenesis imperfecta (OI) is a heritable connective tissue disorder that is clinically characterized by bone fragility, long-bone deformity, scoliosis, blue or blue-gray sclera and dentinogenesis imperfecta [1]. In 90% of patients, OI is caused by mutations in *COL1A1* or *COL1A2* leading to a structural defect of the bone matrix protein collagen type I [2]. Our clinical studies have shown that individuals with OI have reduced muscle mass and function and that these muscle deficits correlated with surrogate measures of bone mass and strength [3,4]. As muscle and bone mass are closely correlated during development, this led to the hypothesis that correction of the muscle deficit could also have a beneficial effect on bone in OI [5].

During muscle growth, myostatin and activin A play a crucial role. Both factors are members of the TGF-β super family that not only act as predominantly negative regulators of muscle growth, but also affect bone matrix homeostasis [6,7]. Myostatin (encoded by *Mstn*) is produced by muscle cells, whereas activin A, a homodimer of inhibin β_A subunits (encoded by *Inhba*), is formed by bone-forming osteoblasts [8–10]. Both factors mediate their signals via the receptors activin receptor type IIB (ActRIIB) and ALK4,5 or 7 [11,12] and intracellular via Smad2 and 3 proteins, which in turn regulate specific gene expression. Myostatin knockout mice (*Mstn*−/−) have muscle hypertrophy and hyperplasia as well as increased bone mass and biomechanical strength [13,14]. Activin A knockout mice (*Inhba*−/−)die in the neonatal period due to tooth and palate defects [15].

When heterozygous *oim* mice, a model of mild OI, were made genetically myostatin deficient, they had increased skeletal muscle mass and increased bone volume and strength [16]. A pharmacological method to inhibit myostatin (and activin A) signaling is to systemically inject a soluble activin receptor type IIB (ActRIIB)-mFc fusion protein. This approach has been assessed in the homozygous *oim* mouse, a model of severe recessive OI with spontaneous fractures and the heterozygous +/*G610C* mouse, a milder model of dominant OI that does not develop spontaneous fractures. Both models revealed improved muscle mass and trabecular bone volume after ActRIIB-mFc-treatment but only improved diaphyseal bone geometry in +/*G610C* mice [17–19]. This suggests differences in treatment response attributed to OI severity.

In the present study we therefore examined the effect of anActRIIB-

* Corresponding author at: Shriners Hospital for Children, 1003 Boulevard Decarie, Montreal, Quebec H4A 0A9, Canada.
E-mail address: frauch@shriners.mcgill.ca (F. Rauch).

https://doi.org/10.1016/j.bone.2019.115036
Received 17 June 2019; Received in revised form 10 August 2019; Accepted 12 August 2019
Available online 13 August 2019

mFc-treatment in a dominant OI mouse model with spontaneous fractures, the *Col1a1*$^{Jrt/+}$ mouse. The *Col1a1*$^{Jrt/+}$ mouse harbors a splice site mutation in the *COL1A1* gene, leading to an 18-amino acid deletion in the collagen type I α1 chain [20]. *Col1a1*$^{Jrt/+}$mice aresmaller in size and develop spontaneous fractures. They have lower bone volume/tissue volume (BV/TV) in trabecular bone, as well as reduced muscle mass [20]. We assessed whether ActRIIB-mFcis effective in improving muscle mass and bone mass and strength in the *Col1a1*$^{Jrt/+}$mouse.

2. Material and methods

2.1. Animals

All experiments were approved by the Animal Care Committee of McGill University and conformed to the ethical guidelines of the Canadian Council on Animal Care. The *Col1a1*$^{Jrt/+}$mice on an FVB background, developed by screening of N-ethyl-N-nitrosourea-induced mutagenesis [20] were a gift from Dr. Jane Aubin's laboratory, University of Toronto, Canada. The breeding colony was maintained at the Animal Care Facility of the Shriners Hospitals for Children-Canada. Animals were on a 12-h alternating light and dark cycle and had unrestricted access to water and food (Charles River rodent diet #5075).

2.2. ACE-2494 treatment and sample collection

Male wild-type (WT) and *Col1a1*$^{Jrt/+}$mice were randomly assigned to treatment with a soluble activin receptor type IIB fusion protein (ACE-2494; generously provided by Acceleron Pharma, Boston, Massachusetts, USA) or control (tris-saline injections), starting at an age of 8 weeks (n = 8 mice per group). ACE-2494 at doses of 3 or 10 mg per kg body weight was injected twice per week and control solution was injected once a week subcutaneously over a period of 4 weeks. Body weights were recorded at the time of each injection. Mice were euthanized at the end of the 4-week intervention period (at the age of 12 weeks). Blood samples were collected at euthanasia by intracardiac puncture, and serum was separated by centrifugation and stored at −80 °C until analysis.

The quadriceps (QC), gastrocnemius (GA), soleus (SOL), extensor digitorumlongus (EDL), and tibialis anterior (TA) muscles of the right and left leg were isolated and weighted. Muscles of the left leg were snap frozen in liquid nitrogen and stored at −80 °C until further analysis. Muscles of the right leg were prepared for immunohistological analysis of muscle fiber composition.

Femoral length was measured with a digital caliper. Right femurs were collected for micro-computed tomography (microCT) and three-point bending test. Samples were stored at −20 °C in phosphate buffered saline-soaked gauze until testing. Left femurs and lumbar vertebra 1 to 5 were collected for dynamic histomorphometric analysis. For dynamic histomorphometric analysis of the bone, each mouse had received two intraperitoneal injections of calcein (25 mg per kg body weight) at 5 days and at 2 days before sacrifice.

2.3. Immunohistological analysis of muscle fiber composition

Isolated muscles were immersed in successive phosphate-buffered saline (PBS) baths containing increasing concentrations of sucrose (4%, 15%, and 30%). Muscles were then embedded in optimal cutting temperature compound (OCT): 30% sucrose (Shandon Cryomatrix; Thermo Fisher Scientific, Waltham, USA), flash-frozen in isopentane chilled in liquid nitrogen, and stored at −80 °C until analysis. Frozen muscles were then embedded vertically in OCT blocks and eight-micrometer sections were cut beginning at the midpoint of the muscles using a cryostat (CryoStar NX70; Thermo Fisher Scientific). Sections were stored at −80 °C until further analysis.

For immunostaining, muscle sections were thawed and air dried for 30 min at room temperature. Muscle sections were then fixed with 4% paraformaldehyde at 4 °C for 10 min, washed 3 times in PBS for 5 min, followed by a blocking step with 10% goat serum (Invitrogen, CA, USA) for 1 h at room temperature. Next, sections were incubated with primary antibody cocktail containing mouse anti-major histocompatibility complex class I (MHC1) (1: 25; BA-F8, DSHB, Iowa City, IA, USA), mouse anti-major histocompatibility complex class IIa (MHCIIa) (1:200; SC-71, DSHB), mouse anti- major histocompatibility complex class IIb (MHC2b) (1:200; BF-F3, DSHB), and rabbit anti-laminin (1:750, #L9393; Sigma, USA) overnight at room temperature. After three 5-min rinses in PBS, sections were incubated with secondary antibody cocktail containing Alexa Fluor® 350 goat anti-mouse IgG (1:500), Alexa Fluor® 594 goat anti-mouse IgG (1:100), Alexa Fluor® 488 goat anti-mouse IgG (1:500), and Alexa Fluor® 488 goat anti-rabbit IgG (1:500) (Invitrogen, CA, USA) for 1 h at room temperature. Subsequently, sections were washed 3 times for 5 min each in PBS and were covered with mounting medium (ProLong ® Gold antifade reagent, Life technologies) and a coverslip. Samples in which the primary antibodies were omitted served as controls.

Pictures of the stained muscle sections were taken using a Leica DMRB fluorescence microscope (Leica Camera, Wetzlar, Germany) equipped with an Olympus DP70 digital camera (Olympus Optical Co., Tokyo, Japan), PhotoFluor LM-75 lamp (89'North, Burlington, Canada), 10×/0.30 PL FLUOTAR objective (Leica Camera, Wetzlar, Germany), and the DP controller software (Version 2.2.1.227, Olympus Corporation).Using freely available Image J software (Version 1.51j) the following parameters were measured: myofiber total number and total area (TA), cross-sectional area (CSA), perimeter, minimal diameter of every myofiber, and number of myofiber types.

Table 1
Relative muscle mass (mg per g of body mass) of male WT and male *Col1a1*$^{Jrt/+}$ mice at 8 weeks of age.

	WT	Col1a1$^{Jrt/+}$
Body mass (g)	24.5 (0.53)	13.7 (0.56)***
Quadriceps (mg/g)	6.29 (0.17)	5.72 (0.22)*
Gastrocnemius (mg/g)	4.67 (0.10)	3.99 (0.23)**
Tibialis anterior (mg/g)	1.78 (0.07)	1.33 (0.06)*
EDL (mg/g)	0.68 (0.07)	0.48 (0.05)*
Soleus (mg/g)	0.59 (0.10)	0.33 (0.05)*

N = 8 mice per group. Values represent mean (SEM).
* Differences between genotypes were tested for statistical significance using the unpaired t-test $p < 0.05$
** Differences between genotypes were tested for statistical significance using the unpaired t-test $p < 0.01$.
*** Differences between genotypes were tested for statistical significance using the unpaired t-test $p < 0.001$.

2.4. Micro-computed tomography

Micro-computed tomography of the right femurs was performed using Skyscan 1272 at a voxel size of 5 μm. Scan parameters included a 0.40-degree increment angle, 3 frames averaged, a 66 kV and 142-mA X-ray source with a 0.5-mm Al filter to reduce beam-hardening artefacts. Trabecular bone was analyzed in a region starting at 0.5 mm proximal of the distal femoral growth plate (to avoid primary spongiosa) and scanning a 1.0 mm section of bone in a proximal direction. Trabecular bone was manually selected along the inner cortical surface. Scans were quantified using the system's analysis software (Skyscan CT Analyser, Version 1.16.1.0). To analyze cortical bone, scanning was performed starting at 44% of the total femur length from the distal end and scanned for 1 mm proximally. The software derivesouter bone diameter and the diameter of the bone marrow cavity from cross-sectional areas using a circular bone cross-section model. Cortical thickness is calculated as the difference of these two diameters divided by 2.

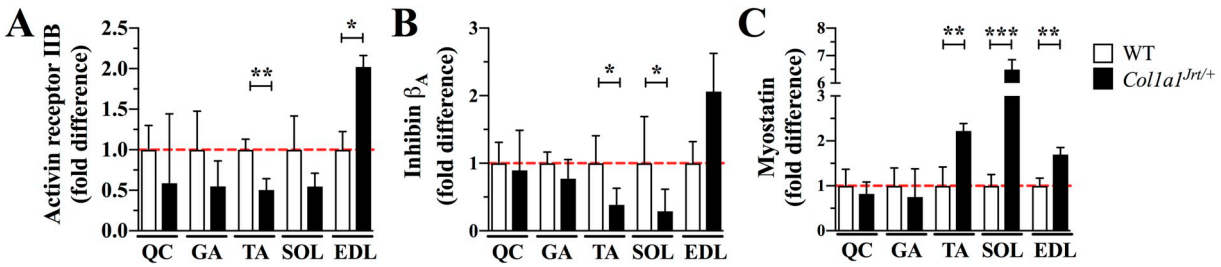

Fig. 1. Gene expression in muscles of 8-week old mice. (A) activin receptor IIb, (B) inhibin β_A, (C) myostatin. Data represent mean ± SEM. $n = 4$ to 5 mice per group. Gene expression normalised to 18S and age-related WT animals, representing fold difference in gene expression of OI samples relative to WT samples. QC, quadriceps; GA, gastrocnemius; TA, tibialis anterior; EDL, extensor digitorum longus; SOL, soleus. Differences between genotypes were assessed for statistical significance using one-way ANOVA, with Bonferroni adjustment for post-hoc tests: $*p < 0.05$, $**p < 0.01$, $***p < 0.001$.

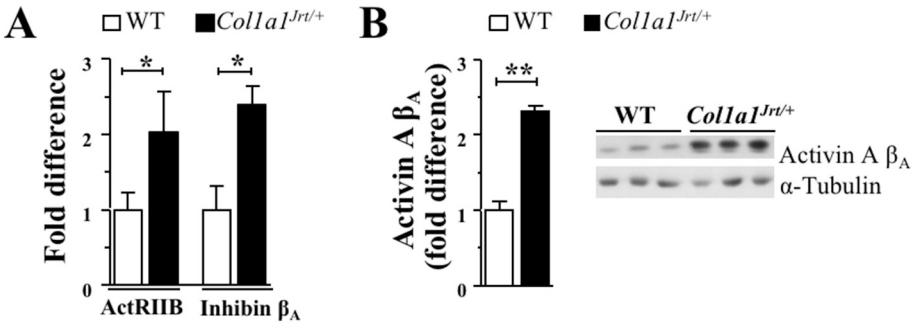

Fig. 2. Baseline results in calvaria of 8-week old mice.(A) Gene expression analysis of activin receptor IIB and inhibin β_A. (B) Protein quantification of activin A. Data represent mean ± SEM. $N = 4$–5 mice per group. (A) Gene expression normalised to 18S, representing fold difference relative to WT samples. (B) Quantification of Western blot analysis of activin A subunit β_A and α-tubulin levels in calvaria of WT and *Col1a1*$^{Jrt/+}$ samples. Differences between *Col1a1*$^{Jrt/+}$ and WT groups were assessed by unpaired *T*-Test: $*p < 0.05$, $**p < 0.01$.

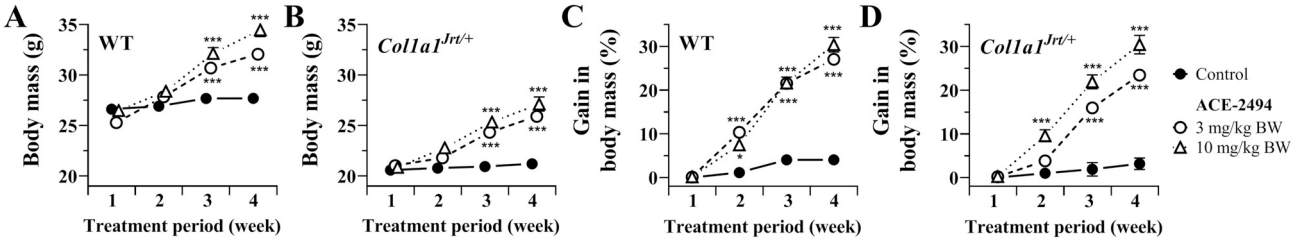

Fig. 3. Body mass during the 4-week treatment period. (A, B) Absolute body mass. (C, D) Body mass gain expressed as percentage change from baseline. Values presented as mean ± SEM. $N = 8$ mice per group. Differences between control group and ACE-treatment of the same genotype were assessed for statistical significance using two-way ANOVA with Bonferroni adjustment for post-hoc tests: $*p < 0.05$, $**p < 0.01$, $***p < 0.001$.

Table 2
Relative muscle mass (mg per g of body mass) of WT and *Col1a1*$^{Jrt/+}$ mice at the end of the ACE-2494 intervention period.

		WT			Col1a1$^{Jrt/+}$		
		Control	ACE-2494 (mg/kg)		Control	ACE-2494 (mg/kg)	
			3	10		3	10
Quadriceps	mg/g	6.95 (0.20)	8.14 (0.19)***	8.34 (0.18)***	6.36 (0.25)	6.91 (0.18)	7.06 (0.22)
Gastoc-nemicus	mg/g	5.33 (0.12)	5.88 (0.12)**	5.97 (0.09)***	4.81 (0.09)	5.38 (0.13)**	5.88 (0.13)***
Tibialis anterior	mg/g	1.56 (0.04)	1.90 (0.05)***	2.02 (0.04)***	1.39 (0.03)	1.79 (0.04)***	1.83 (0.06)***
EDL	mg/g	0.29 (0.02)	0.33 (0.03)	0.40 (0.01)**	0.34 (0.02)	0.48 (0.03)***	0.43 (0.02)
Soleus	mg/g	0.23 (0.02)	0.23 (0.01)	0.24 (0.01)	0.18 (0.01)	0.25 (0.02)**	0.22 (0.01)

Values presented as mean (SEM). $N = 16$ (N = 8 muscle of the left leg; N = 8 muscle of the right leg) per group. Differences between treatment groups of the same genotype were assessed by One-way ANOVA with Bonferroni post-test and are indicated by asterisks.
** $p < 0.01$.
*** $p < 0.001$.

2.5. Three-point bending test

Following micro-computed tomography scanning, right femora were loaded to failure in three-point bending using a Materials Testing System Model 5943 (INSTRON, Norwood, MA, USA). The specimens were thawed one day prior to the test and all muscle tissues were cleaned off. The bone was soaked overnight in PBS at room temperature until mechanical testing. The distance between the lower supports was 7 mm with a vertical displacement rate of 50 µm/s. The anterior mid-diaphysis was loaded under tension. Test results were analyzed using the system's analysis software Bluehill (Illinois Tool Works Inc., Glenview, IL, USA; Version 3.65).

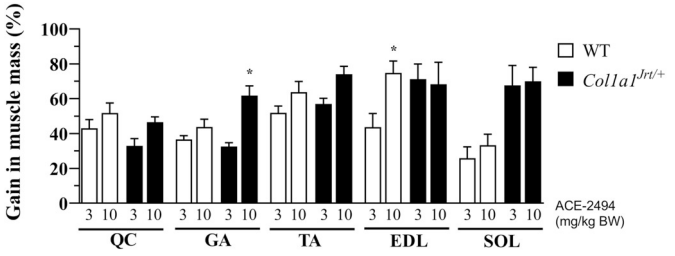

Fig. 4. Gain in muscle mass of ACE-2494 treated mice expressed as percent difference relative to the muscle mass of vehicle-treated mice of the same genotype. Values presented as mean ± SEM. $N = 8$ mice per group, QC, quadriceps; GA, gastrocnemius; TA, tibialis anterior; EDL, extensor digitorumlongus; SOL, soleus; 3, 3 mg per kg body mass ACE-2494; 10, 10 mg per kg body mass ACE-2494. Differences between dose of ACE-2494 of the same genotype were assessed for statistical significance using one-way ANOVA with Bonferroni adjustment for post-hoc tests: $^{*}p < 0.05$, $^{**}p < 0.01$, $^{***}p < 0.001$.

2.6. Serum bone markers

Serum levels of total calcium, inorganic phosphorus, and alkaline phosphatase were determined by standard methods (McGill Diagnostic Laboratory, Montreal, Canada). Markers of bone formation (procollagen type I N-terminal propeptide, PINP; Mouse/Rat PINP, Immunodiagnostic Systems) and of bone resorption (C-telopeptide of collagen type I, CTX; RatLaps, Immunodiagnostic Systems) as well as serum levels of myostatin (DAC00B; R&D Systems) and activin A (DGDF80; R&D Systems) were quantified by enzyme immunoassays. Serum tests were performed in duplicate.

2.7. Bone histomorphometry

Histomorphometric analysis of trabecular bone was performed at the left distal femur (starting at 50 µm proximal to the growth plate to a distance of 1.4 mm from the growth plate) and in lumbar vertebra 4 (L4, entire trabecular compartment). Specimens were fixed in 10% phosphate-buffered formalin, dehydrated in increasing concentrations of ethanol and embedded in methylmethacrylate. Undecalcified 6 µm thick sections were cut with a Polycut E microtome (Reichert-Jung, Heidelberg, Germany). The sections were deplastified with ethylene glycol monoethyl acetate to allow for optimal staining. In each sample, two consecutive sections were selected that were stained with Masson Goldner Trichrome for static parameters or mounted unstained for the measurement of dynamic parameters using fluorescence microscopy.

Histomorphometric measurements in mice were carried out using a digitizing table with Osteomeasure® software (Osteometrics Inc., Atlanta, GA, USA). In addition to standard histomorphometric parameters, we measured cartilage volume per bone volume. This represents the relative amount of growth plate material within secondary trabeculae. Nomenclature and abbreviations follow the recommendations of the American Society for Bone and Mineral Research [21].

2.8. Quantitative real-time RT-PCR

Total RNA was isolated from snap-frozen tissue samples by using TRIzol™ (ThermoFisher Scientific, Waltham, USA) according to the manufacturer's protocol. Reverse transcription of 1 µg RNA was performed using the High Capacity cDNA Reverse Transcription Kit (Applied Biosystems, ThermoFisher Scientific, Waltham, USA). Real-time PCR was performed with 50 ng of cDNA using a QuantStudio™ 7 Flex System (ThermoFisher Scientific, Waltham, USA), TaqMan™ Fast Advanced master mix (4,444,557, ThermoFisher Scientific, Waltham, USA) and the following FAM labelled TaqMan® gene expression primers: Mstn (Mm01254559), ActRIIB (Mm00431664), Inhibin β_A (Mm00434339), and 18S (Mm03928990) was used as endogenous control. Gene expression was analyzed according to the delta-delta Ct method.

2.9. Western blot

Total protein was isolated from snap-frozen tissue samples by using TRIzol™ (ThermoFisher Scientific, Waltham, USA) according to the manufacturer's protocol. Protein concentration was measured using Pierce™ BCA Protein Assay Kit (ThermoFisher Scientific, Waltham, USA) following the manufacturer's directions. 40 µg of protein extracts were separated by SDS-Page (12.5%) and transferred onto nitrocellulose membrane (0.45 µm, Bio-Rad Laboratories, Hercules, USA) for Western blot analyses. Nitrocellulose membranes were incubated with Human/Mouse/Rat Activin A βA subunit (#AF338, R&D Systems, Minnesota, USA) at a dilution of 1:1000 in Tris-buffered saline/0.05% Tween 20 containing 5% bovine serum albumin overnight at 4 °C, followed by secondary horseradish peroxidase-linked anti-goat antibody (#HAF017, R&D Systems, Minnesota, USA) at a dilution of 1: 2000 in TBST containing 5% BSA for 2 h. Expression was detected with ECL Plus Western Blotting Detection System (GE, Boston, USA) and X-ray films. Subsequently, antibody was stripped from membranes using stripping buffer (20 mM Tris pH 7.5, 10 mM DTT, 7 M guanidine hydrochloride, 20 min at room temperature) and re-incubated with α-tubulin monoclonal antibody at a dilution of 1:10,000 in TBST containing 5% BSA for 1 h (#T6074; Sigma-Aldrich, St. Louis, USA), followed by similar secondary antibody incubation and ECL-mediated visualization. X-ray films were scanned, and the density of each band was quantified using ImageJ2 software [22].

2.10. Statistics

Unless stated otherwise, data presented here are shown as mean ± SEM. Differences between treatment groups of the same genotype were assessed by one-way ANOVA with Bonferroni post-test

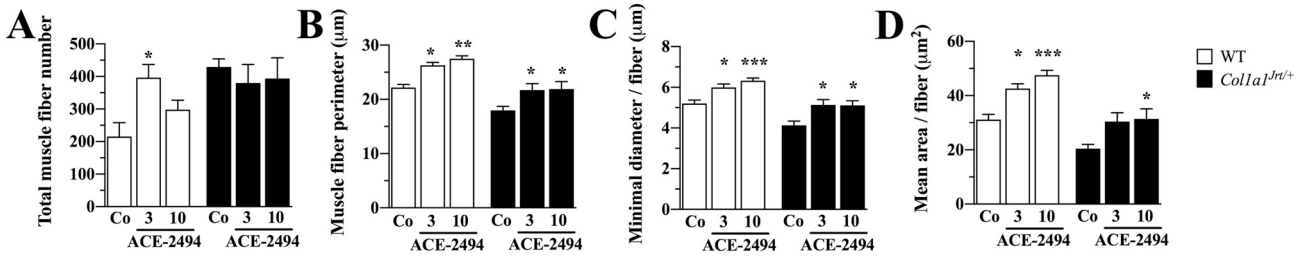

Fig. 5. Effect of ACE-2494 on soleus muscle fibers. (A) Total number of muscle fibers. (B) Muscle fiber perimeter. (C) Muscle fibers diameter. (D) Mean muscle fiber cross-sectional area. $N = 7$ to 8 per group. Values presented as mean ± SEM. Co, Control-treated cohort.3, 3 mg per kg body mass ACE-2494; 10, 10 mg per kg body mass ACE-2494. Differences between treatment groups of the same genotype were assessed for statistical significance using one-way ANOVA, with Bonferroni adjustment for post-hoc tests: $^{*}p < 0.05$, $^{**}p < 0.01$, $^{***}p < 0.001$.

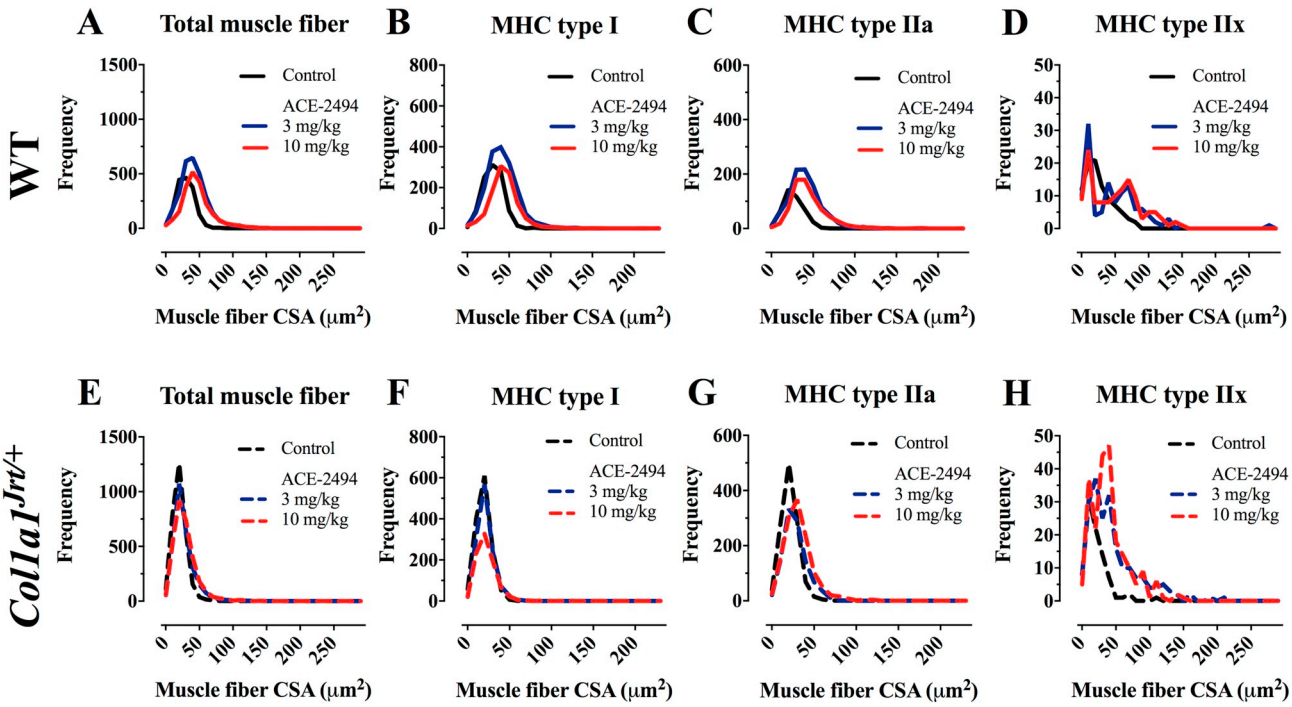

Fig. 6. Muscle fiber size distribution in soleus muscle. (A) All fibers. (B) Type I fibers. (C) Type IIa fibers. (D) Type IIx fibers. N = 7 to 8 mice per group. Differences between treatment groups of the same genotype were assessed for statistical significance using one-way ANOVA, with Bonferroni adjustment for post-hoc tests. In WT and *Col1a1*$^{Jrt/+}$ cohorts fiber size distribution was significantly different ($p < 0.01$) in ACE-2494 treated cohorts compared to control-treated cohorts for each fiber type.

using GraphPad Prism version 7.0d (GraphPad Software, San Diego, California, USA). $P < 0.05$ was considered significant.

3. Results

At 8 weeks of age, *Col1a1*$^{Jrt/+}$ mice had significantly higher activin A serum levels than WT littermates (73 ± 8 pg/mL vs. 50 ± 5 pg/mL; $P = 0.02$; $n = 4$–5 per genotype), whereas serum levels of total myostatin were similar between genotypes (7.3 ± 1.7 pg/mL vs. 6.8 ± 1.3 pg/mL; $P = 0.81$; n = 4–5 per genotype). Muscle mass was significantly lower in *Col1a1*$^{Jrt/+}$ mice than in WT littermates (Table 1).

Compared to WT mice, *Col1a1*$^{Jrt/+}$ mice had higher myostatin gene expression in TA, SOL, and EDL, whereas differences in ActRIIB and inhibin $\beta_A$gene expression varied between muscles (Fig. 1).

Analysis of calvaria bone tissue revealed that*Col1a1*$^{Jrt/+}$ mice expressed higher levels of ActRIIB and inhibin β_A (Fig. 2A) and had significantly elevated activin A proteins levels (Fig. 2B), suggesting increased ActRIIB signaling in bone.

At 8 weeks of age, the body mass of *Col1a1*$^{Jrt/+}$ mice was approximately 45% lower than of WT littermates. This difference persisted during treatment with ACE-2494,as both genotypes had similar gains in body mass (Fig. 3 A-D).

The treatment was also associated with a significant dose-dependent increase in muscle mass in both groups of mice (Table 2). Compared to control-treated groups, ACE-2494 treated WT and *Col1a1*$^{Jrt/+}$ mice gained 30% to 75% muscle mass, with the largest gains observed in EDL and SOL of *Col1a1*$^{Jrt/+}$mice (Fig. 4). No adverse side effects of ACE-2494 treatment were observed.

Myofiber analysis of SOL muscle revealed that control-treated *Col1a1*$^{Jrt/+}$ mice had more but smaller myofibers than WT littermates (Fig. 5). This was true for both slow and fast twitch myofibers (MHC I and IIa) (Fig. 6A–D). ACE-2494 treatment was associated with a dose-dependent increase in muscle fiber size in both WT and *Col1a1*$^{Jrt/+}$ mice (Fig. 5B–D, Fig. 6B–D).

Control-treated *Col1a1*$^{Jrt/+}$ mice had a lower proportion of slow-twitch myofibers (MHC I) but a higher proportion of fast twitch myofibers (MHC IIa) and slow-fast myofiber hybrids (MHC I/IIA) than WT littermates (Fig. 7A–D). ACE-2494 treatment resulted in a dose-dependent reduction of slow-twitch myofibers in WT and *Col1a1*$^{Jrt/+}$ mice, but an increase in fast twitch myofibers in WT and slow-fast myofiber hybrids in *Col1a1*$^{Jrt/+}$ mice (Fig. 7A–F).

At sacrifice, healed femur fractures were observed in one control-treated *Col1a1*$^{Jrt/+}$ mouse, one *Col1a1*$^{Jrt/+}$ mouse in the 3 mg/kg ACE-2494 group and two *Col1a1*$^{Jrt/+}$ mice receiving 10 mg/kg ACE-2494. These femur specimens were excluded from femoral length measurement, micro-computed tomography analysis, 3-point-bending test, and histomorphometric analysis. Treated WT littermates had no detectable abnormalities of the long bones or other organs after ACE-2494 treatment.

In both WT and *Col1a1*$^{Jrt/+}$ mice, ACE-2494 was associated with a dose-dependent increase in femoral length. Distal femoral trabecular BV/TV and trabecular number increased only in WT mice (Fig. 8). Even though cortical thickness did not change with ACE-2494 in either genotype, periosteal and endocortical diameter increased significantly in *Col1a1*$^{Jrt/+}$ mice, leading to improved polar moment of inertia (Fig. 8F–H). However, maximal and fracture load increased in ACE-2494-treated WT mice but not in *Col1a1*$^{Jrt/+}$ mice (Fig. 8I–L). In L4 vertebra, ACE-2494 had no effect on trabecular BV/TV or bone formation rate in either genotype (Table 3).

Serum levels of activin A were higher in control-treated *Col1a1*$^{Jrt/+}$ mice than in control-treated WT. ACE-2494 purged activin A from the serum in both genotypes (Table 4). ACE-2494 treatment was also associated with significantly higher osteoclast numbers in WT and *Col1a1*$^{Jrt/+}$ mice (TRAP, Table 4). Serum CTX-I levels increased significantly in *Col1a1*$^{Jrt/+}$ mice (Table 4). Bone formation markers (P1NP and alkaline phosphatase), as well as serum calcium levels and phosphorus levels, were not affected by ACE-2494 (Table 4). Further, ACE-2494 at a dose of 10 mg/kg significantly increased insulin levels whereas glucose levels were not affected (Table 4).

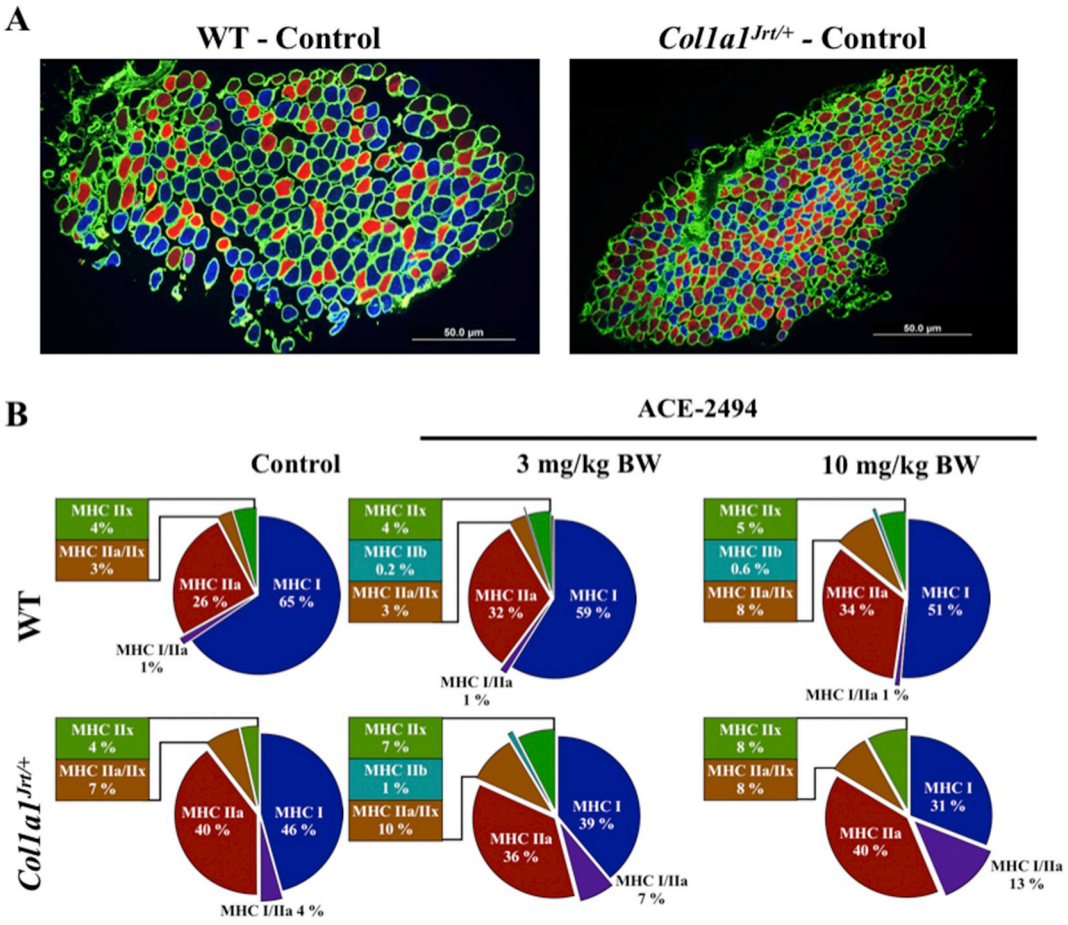

Fig. 7. Myofiber composition in soleus muscle. (A) Representative images of immunohistochemical staining of soleus muscle in control-treated wild type and *Col1a1*$^{Jrt/+}$ mice. (B) Quantification of muscle fiber distribution in wild type and *Col1a1*$^{Jrt/+}$ mice. N = 7 to 8 per group. Values presented as mean. Differences between treatment groups of the same genotype were assessed for statistical significance using one-way ANOVA, with Bonferroni adjustment for post-hoc tests. In wild type, ACE-2494 10 mg/kg BW significantly reduced MHC I fiber types ($P < 0.01$) and significantly increased MHC IIa fiber types ($P < 0.001$). In *Col1a1*$^{Jrt/+}$, ACE-2494 10 mg/kg BW significantly reduced MHC I fiber types ($P < 0.01$) and increased fiber hybrids.

4. Discussion

In this study we found that compared to WT littermates, 8-week old *Col1a1*$^{Jrt/+}$ mice have significantly elevated activin A serum levels, increased myostatin gene expression in muscle tissue, lower muscle mass during development, as well as higher ActRIIB signaling in bone. Treatment of *Col1a1*$^{Jrt/+}$ mice with ACE-2494 improved muscle mass and bone geometry of the femoral diaphysis. In WT mice, ACE-2494 treatment was associated with improved muscle and bone mass.

The muscle mass phenotype in *Col1a1*$^{Jrt/+}$ mice is in accordance with the observation in inhibin A-deficient mice (*inha*$-/-$), a negative regulator of activin A, that activin A serum levels directly correlate with muscle wasting [23]. Activin A and myostatin are both negative regulators of muscle mass and inhibition of these ligands simultaneously results in synergistical muscle mass growth [9]. As shown in mouse models of OI [17,19], Duchenne Muscular Dystrophy [24], or WT C57BL/6 mice [25], ACE-2494 treatment in *Col1a1*$^{Jrt/+}$ mice results in a dose-dependent increase in muscle mass due to myofiber hypertrophy.

In addition, our data demonstrate that ACE-2494-induced myofiber hypertrophy coincidied with modified myofiber composition. In WT mice, slow contractile myofibers (MHC I) transitioned to more potent fast contractile myofibers (MHC IIa), whereas in *Col1a1*$^{Jrt/+}$ mice these myofibers transitioned to myofiber hybrid forms (MHC I/IIa, MHC IIx/IIb). Myofiber transition is known to take place in response to exercise, based on the adaptation of myofiber metabolism, and physiological and contractile properties of skeletal muscle [26]. Whether the increase in muscle mass translates into improved movement of *Col1a1*$^{Jrt/+}$ and WT mice leading to myofiber transition, will be an important topic for the future.

Interestingly, studies in *oim/oim* and *+/G610C* mice found that trabecular number increased after ActRIIB-mFc treatment [17,18]. While we used a similar treatment protocol (20 mg/kg per body weight per week), ACE-2494 treatment did not change trabecular bone volume in *Col1a1*$^{Jrt/+}$ mice. It was shown that activin A induces osteoclast differentiation in vitro and in vivo [27–30], although some reports suggest a negative effect on the survival of mature osteoclasts [31]. Myostatin may directly regulate osteoclast differentiation [6]. In the present study ACE-2494 treatment resulted in increased TRAP serum levels in both WT and *Col1a1*$^{Jrt/+}$ mice, suggesting an elevated number of osteoclasts but significantly increased bone resorption, as indicated by CTX-I serum levels, in ACE-2494-treated *Col1a1*$^{Jrt/+}$ mice at 10 mg/kg body weight only. This is in line with increased osteoclast numbers in aged *Mstn*$-/-$ mice [7] and elevated CTX-I serum levels in ActRIIB-mFc-treated OI mouse models, *+/G610C* and *oim/oim*, beside increased trabecular number [18].

ActRIIB-mFc treatment resulted in a dose-dependent increase in insulin levels in WT and *Col1a1*$^{Jrt/+}$ mice while glucose levels were not affected. So far, one study in juvenile rhesus macaques reported about unaffected glucose levels after intervention with ActRIIB-mFc [32]. Activins are expressed by pancreatic islet cells and are involved in glucose/energy metabolism by regulating islet cell proliferation/

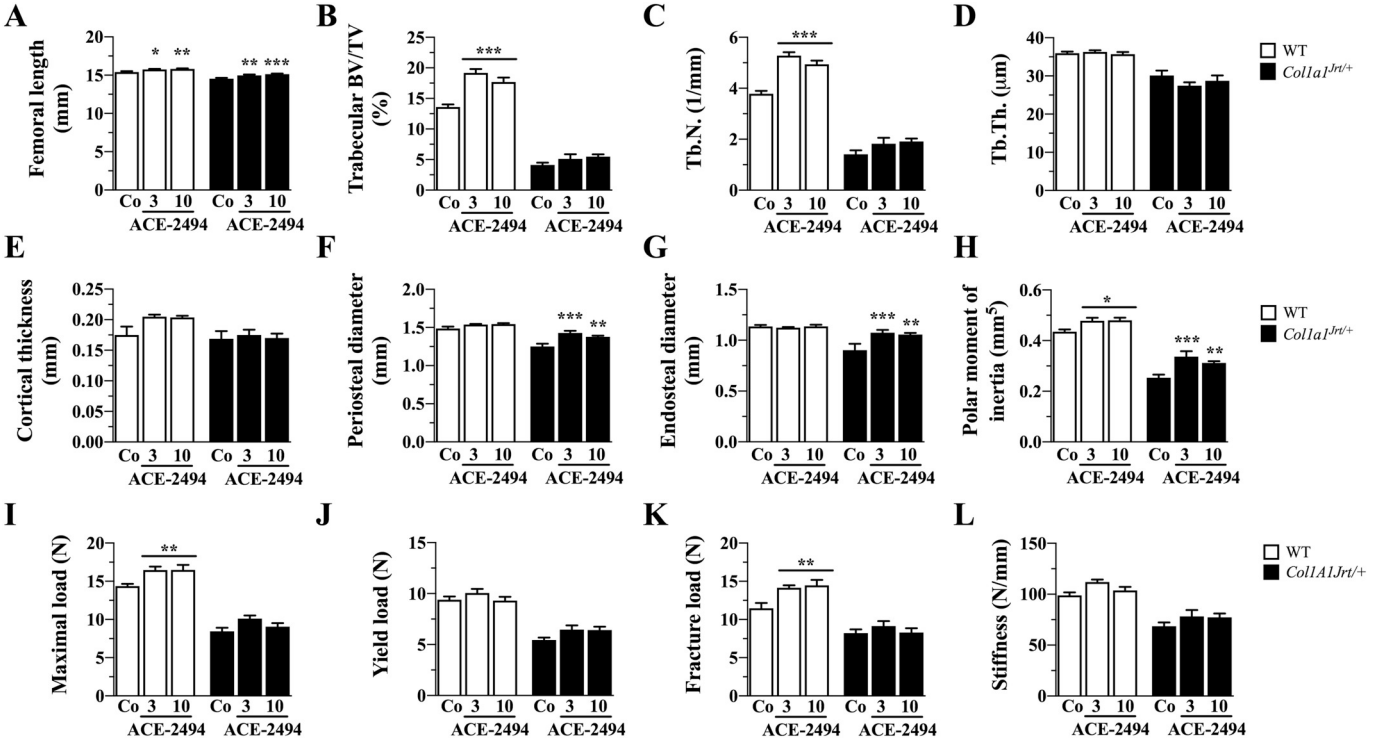

Fig. 8. Analysis of femur structure and mechanical properties. (A–D) Trabecular bone assessment by microCT in the distal metaphysis. (E–H) Cortical bone assessment by microCT at the mid-shaft diaphysis. (I–L) Results of three-point bending tests. $N = 6–8$ mice per group; Values presented as mean ± SEM. Co, Control-treated cohort. Differences between treatment groups of the same genotype were assessed for statistical significance using one-way ANOVA, with Bonferroni adjustment for post-hoc tests: *p < 0.05, **p < 0.01, ***$p < 0.001$.

Table 3
Results of bone histomorphometry of lumbar vertebra L4 at the end of the intervention period.

	WT			Col1a1$^{Jrt/+}$		
	Control	ACE-2494 (mg/kg)		Control	ACE-2494 (mg/kg)	
		3	10		3	10
BV/TV (%)	13.9 (1.2)	14.1 (1.0)	15.5 (1.2)	3.7 (0.5)	4.8 (1.2)	4.3 (0.7)
Tb.N (1/mm)	3.9 (0.3)	3.9 (0.3)	4.2 (0.3)	1.6 (0.1)	1.8 (0.3)	1.6 (0.1)
Tb.Th (µm)	35.4 (1.5)	37.3 (2.9)	37.3 (1.1)	23.3 (1.9)	25.5 (1.7)	26.9 (2.1)
BFR/BS (µm^3/µm^2 * y)	64.1 (7.7)	65.5 (4.9)	63.5 (7.6)	40.5 (6.6)	25.9 (4.0)	32.1 (6.9)
MAR (µm/d)	1.2 (0.06)	1.1 (0.05)	1.1 (0.1)	0.9 (0.02)	0.7 (0.07)	0.8 (0.1)
MS/BS (%)	14.9 (1.3)	15.9 (0.8)	15.6 (1.5)	12.0 (2.0)	8.7 (1.1)	9.1 (1.7)

N = 7 to 8 mice per group; Values represent mean (SEM). Differences between treatment groups of the same genotype were assessed using one-way ANOVA, with Bonferroni adjustment for post-hoc tests. No statistical differences were found.

differentiation and insulin production, and tissue-specific insulin sensitivity [33]. For example, activin B suppresses insulin secretion [34] indicating that binding by ActRIIB-mFc [35] antagonizes this effect leading to increased levels in insulin.

Despite trabecular bone, ActRIIB-mFctreatment led onlyin +/*G610C* mice to increased cortical cross-sectional area and improved biomechanical bone properties [18]. ACE-2494 treatment also improved bone geometry in *Col1a1*$^{Jrt/+}$ mice but did notresult in enhanced biomechanical properties. In +/*G610C* mice observed periosteal bone growth was suggested to relay on an anabolic response of periosteal osteoblast [18] since inhibition of activin and/or myostatin have a direct or indirect effecton osteoblasts [36–38]. Additionally it was shown that activin A alters extracellular matrix composition by regulating gene expression of extracellular matrix proteins and cell-matrix adhesion [39] or by impairing matrix vesicle production in mineralizing osteoblasts [10]. However, differences in biomechanical response in different OI mouse models are probably due to the different composition of the extracellular bone matrix due to different collagen mutations, leading to either a mild bone phenotype of OI like +/*G610C* mice or more moderate to severe form like in *oim/oim* and *Col1a1*$^{Jrt/+}$ mice.

Although ACE-2494 treatment failed to correct the trabecular bone phenotype of *Col1a1*$^{Jrt/+}$ mice, the intervention was associated with increased femoral length in *Col1a1*$^{Jrt/+}$ and WT mice. This effect was also reported in +/*G610C* mice but not in *oim/oim* mice after ActRIIB-mFc treatment [18]. This suggests a positive effect of ACE-2494 on epiphyseal growth plate cartilage. Previous studies demonstrated that proliferating and hypertrophic chondrocytes and osteoblasts express activin, activin receptor I, and activin receptor II [40] and that activin A suppresses chondrocyte differentiation [41] and myostatin chondrocyte proliferation [42]. Interestingly, it was further shown that the multi-differentiation potential of mesenchymal progenitor cells correlates with activin A levels and/or activin A: follistatin ratio and that activin A is required for the chondrogenic and osteogenic differentiation of mesenchymal progenitor cells [43]. The growth plate also responds to signals via the growth hormone/insulin like growth factor I axis which

Table 4
Serum parameters at the end of the intervention period.

	WT			Col1a1^{Jrt}/+		
	Control	ACE-2494 (mg/kg)		Control	ACE-2494 (mg/kg)	
		3	10		3	10
Activin A (pg/mL)	24.5 (3.2	< 0.75***	< 0.75***	43.7 (3.9)	< 0.75***	< 0.75***
CTX (ng/mL)	8.6 (0.3)	9.5 (0.5)	10.9 (0.6)	16.2 (1.4)	19.3 (2.4)	25.2 (1.6)***
TRAP (U/L)	8.9 (0.3)	11.1 (0.1)**	11.4 (0.4)***	8.2 (0.3)	10.3 (0.3)**	9.9 (0.6)*
PINP (ng/mL)	55.9 (1.1)	63.4 (7.9)	57.6 (5.8)	60.2 (6.8)	69.4 (7.3)	64.2 (7.6)
Alkaline Phosphatase (U/L)	118 (4)	128 (6)	119 (7)	128 (6)	121 (9)	128 (5)
RANKL (pg/mL)	156 (2)	102 (15)	72 (32)	82 (13)	93 (7)	109 (32)
Glucose (mmol/L)	14.5 (0.5)	12.8 (0.8)	12.6 (1.0)	10.7 (0.5)	13.8 (1.1)	12.9 (0.8)
Insulin (ng/mL)	0.95 (0.13)	1.12 (0.16)	1.81 (0.21) **	0.39 (0.05)	0.84 (0.16)	0.98 (0.17)*
Calcium (mmol/L)	2.26 (0.02)	2.26 (0.02)	2.31 (0.02)	2.25 (0.03)	2.26 (0.02)	2.26 (0.02)
Inorganic phosphorus (mmol/L)	2.52 (0.06)	2.76 (0.12)	2.68 (0.12)	2.48 (0.05)	2.68 (0.16)	2.83 (0.10)

N = 4 to 8 mice per group. Values represent mean (SEM).
* Differences between treatment groups of the same genotype were assessed by One-way ANOVA with Bonferroni adjustment for post-hoc tests: $p < 0.05$.
** Differences between treatment groups of the same genotype were assessed by One-way ANOVA with Bonferroni adjustment for post-hoc tests: $p < 0.01$.
*** Differences between treatment groups of the same genotype were assessed by One-way ANOVA with Bonferroni adjustment for post-hoc tests: $p < 0.001$.

Table 5
Ligand trap design and in vitro half maximal inhibitory concentrations (IC_{50}).

Ligand trap	hActRIIB-Fc	ACVR2B/Fc	RAP-031[a]	ACE-2494[a]
Reference	[25]	[51]	[52]	[35]
Structure	N-terminal peptide of human ActRIIB fused to human Fc fusion protein	Extracellular domain of murine ActRIIB fused to murine Fc domain	Extracellular domain of ActRIIB fused to mouse IgG2a (Murine version of ACE-031[a])	Structural analog to RAP-031with minimal binding to BMP-9
Myostatin	120 nM[b]	180 pM[c]	322 pM[c]	125 pM[d]
GDF-11	135 nM[b]	180 pM[c]	82 pM[c]	27 pM[d]
Activin	Not reported	1 nM[c]	283 pM[c]	12 pM (activin A and activin B)[d]
Further ligands	Not reported	Not reported	BMP-9	Not reported
Mouse models studied	WT C57BL/6 [25]	oim/oim [17]	+/G610C, oim/oim, Mdx [18,19,24]	WT C57BL/6 [35]

[a] Acceleron Pharma; WT: wild-type.
[b] Applied ligand binding assay: HEK293 β-lactamase assay.
[c] Applied ligand binding assay: $(CAGA)_{12}$-luciferase reporter gene assay.
[d] Biacore T100/T200 biosensor (Biacore/GE Healthcare).

is modulated by activin A [44–46]. Whether modifications inthegrowth hormone/insulin like growth factor I axis might explain some of the results of the present study remains unclear at this point.

We observed healed femoral fractures at sacrifice in ACE-2494-treated *Col1a1*$^{Jrt/+}$mice, similar to what has been reported in *+/G610C* and *oim/oim* mice [18]. As activin A is required for the chondrogenic and osteogenic differentiation, it also plays an important role in bone healing. In a standardized closed tibial fracture mouse model it was shown ActRIIB-Fc treatment significantly increased callus mineralization and improved biomechanical strength [47]. However, here we did not investigate callus properties of healed femoral fractures, which will be an important topic for the future.

ActRIIs have multiple ligands such as activin A, activin B, myostatin, GDF11, BMP9, and BMP10 regulating various biochemical or cellular systems [48]. Different ActRIIB ligand traps vary in their design and thus in their ligand binding properties (Table 5). This may explain some of the differences in treatment outcomes between the present study and published reports on the effects of ActRIIB-ligand trap treatments [17–19,24,25,35]. For example, ActRII-ligand trap ACE-031 neutralizes BMP9/10 leading to vascular side effects [49,50], whereas ACE-2494, a modified version of ACE-031, does not.

Among the limitations of this study is that we studied only male mice at a single time point in their development, 8-weeks of age. It is possible that ACE-2494 treatment at an earlier age could benefit from a synergistic effect of rapid bone growth and muscle mass improvement. It is also possible that there are sex-differences in the response to ACE-2494 as it was shown for *+/G610C* and *oim/oim* mice [18]. Further it is possible that a treatment duration beyond 4 weeks could improve muscle-bone outcomes. So far, the published reports on ActRIIB-ligand trap treatment in OI mice were limited to 4 weeks of treatment in either young adult (8-week old) [18] or adult (12-week old) OI mice [17].

In summary, we demonstrate that ACE-2494 treatment significantly improved muscle mass and diaphyseal bone geometry butdoes not correct trabecular bone phenotype in *Col1a1*$^{Jrt/+}$ mice, a dominant OI mouse model with spontaneous fractures.

Declaration of competing interest

The authors state that they have the following disclosures:
Josephine T. Tauer: None.
Frank Rauch: PreciThera Inc.: Study grant to institution.

Acknowledgments

Supported by Deutsche Forschungsgemeinschaft (TA188/1-2) and the Shriners of North America (84060-CAN-13).

References

[1] A. Forlino, J.C. Marini, Osteogenesis imperfecta, Lancet 387 (10028) (2016) 1657–1671.
[2] G. Bardai, P. Moffatt, F.H. Glorieux, F. Rauch, DNA sequence analysis in 598 individuals with a clinical diagnosis of osteogenesis imperfecta: diagnostic yield and mutation spectrum, Osteoporos. Int. 27 (12) (2016) 3607–3613.
[3] L.N. Veilleux, M. Lemay, A. Pouliot-Laforte, M.S. Cheung, F.H. Glorieux, F. Rauch, Muscle anatomy and dynamic muscle function in osteogenesis imperfecta type I, J.

Clin. Endocrinol. Metab. 99 (2) (2014) E356–E362.
[4] L.N. Veilleux, A. Pouliot-Laforte, M. Lemay, M.S. Cheung, F.H. Glorieux, F. Rauch, The functional muscle-bone unit in patients with osteogenesis imperfecta type I, Bone 79 (2015) 52–57.
[5] L.N. Veilleux, P. Trejo, F. Rauch, Muscle abnormalities in osteogenesis imperfecta, J. Musculoskelet. Neuronal Interact. 17 (2) (2017) 1–7.
[6] B. Dankbar, M. Fennen, D. Brunert, S. Hayer, S. Frank, C. Wehmeyer, D. Beckmann, P. Paruzel, J. Bertrand, K. Redlich, C. Koers-Wunrau, A. Stratis, A. Korb-Pap, T. Pap, Myostatin is a direct regulator of osteoclast differentiation and its inhibition reduces inflammatory joint destruction in mice, Nat. Med. 21 (9) (2015) 1085–1090.
[7] M.W. Hamrick, X. Shi, W. Zhang, C. Pennington, H. Thakore, M. Haque, B. Kang, C.M. Isales, S. Fulzele, K.H. Wenger, Loss of myostatin (GDF8) function increases osteogenic differentiation of bone marrow-derived mesenchymal stem cells but the osteogenic effect is ablated with unloading, Bone 40 (6) (2007) 1544–1553.
[8] J. Rodriguez, B. Vernus, I. Chelh, I. Cassar-Malek, J.C. Gabillard, A. Hadj Sassi, I. Seiliez, B. Picard, A. Bonnieu, Myostatin and the skeletal muscle atrophy and hypertrophy signaling pathways, Cell. Mol. Life Sci. 71 (22) (2014) 4361–4371.
[9] E. Latres, J. Mastaitis, W. Fury, L. Miloscio, J. Trejos, J. Pangilinan, H. Okamoto, K. Cavino, E. Na, A. Papatheodorou, T. Willer, Y. Bai, J. Hae Kim, A. Rafique, S. Jaspers, T. Stitt, A.J. Murphy, G.D. Yancopoulos, J. Gromada, Activin A more prominently regulates muscle mass in primates than does GDF8, Nat. Commun. 8 (2017) 15153.
[10] R.D. Alves, K. Eijken M Fau-Bezstarosti, J.A.A. Bezstarosti K Fau-Demmers, J.P.T.M. Demmers Ja Fau-van Leeuwen, J.P. van Leeuwen, Activin A suppresses osteoblast mineralization capacity by altering extracellular matrix (ECM) composition and impairing matrix vesicle (MV) production, (1535–9484 (Electronic)) (2013).
[11] Z. Huang, X. Chen, D. Chen, Myostatin: a novel insight into its role in metabolism, signal pathways, and expression regulation, Cell. Signal. 23 (9) (2011) 1441–1446.
[12] B. Buehring, N. Binkley, Myostatin—the holy grail for muscle, bone, and fat? Curr Osteoporos Rep 11 (4) (2013) 407–414.
[13] M.W. Hamrick, Increased bone mineral density in the femora of GDF8 knockout mice, Anat Rec A Discov Mol Cell Evol Biol 272 (1) (2003) 388–391.
[14] M.W. Hamrick, T. Samaddar, C. Pennington, J. McCormick, Increased muscle mass with myostatin deficiency improves gains in bone strength with exercise, J. Bone Miner. Res. 21 (3) (2006) 477–483.
[15] M.M. Matzuk, T.R. Kumar, A. Vassalli, J.R. Bickenbach, D.R. Roop, R. Jaenisch, A. Bradley, Functional analysis of activins during mammalian development, Nature 374 (6520) (1995) 354–356.
[16] A.K. Oestreich, S.M. Carleton, X. Yao, B.A. Gentry, C.E. Raw, M. Brown, F.M. Pfeiffer, Y. Wang, C.L. Phillips, Myostatin deficiency partially rescues the bone phenotype of osteogenesis imperfecta model mice, Osteoporos. Int. 27 (1) (2016) 161–170.
[17] D.J. DiGirolamo, V. Singhal, X. Chang, S.J. Lee, E.L. Germain-Lee, Administration of soluble activin receptor 2B increases bone and muscle mass in a mouse model of osteogenesis imperfecta, Bone research 3 (2015) 14042.
[18] Y. Jeong, S.A. Daghlas, X. Yixia, M.A. Hulbert, F.M. Pfeiffer, M.R. Dallas, C.L. Omosule, R.S. Pearsall, S.L. Dallas, C.L. Phillips, Skeletal response to soluble activin receptor type IIB in mouse models of osteogenesis imperfecta, J. Bone Miner. Res. 33 (10) (2018) 1760–1772.
[19] Y. Jeong, S.A. Daghlas, A.S. Kahveci, D. Salamango, B.A. Gentry, M. Brown, R.S. Rector, R.S. Pearsall, C.L. Phillips, Soluble activin receptor type IIB decoy receptor differentially impacts murine osteogenesis imperfecta muscle function, Muscle Nerve 57 (2) (2018) 294–304.
[20] F. Chen, R. Guo, S. Itoh, L. Moreno, E. Rosenthal, T. Zappitelli, R.A. Zirngibl, A. Flenniken, W. Cole, M. Grynpas, L.R. Osborne, W. Vogel, L. Adamson, J. Rossant, J.E. Aubin, First mouse model for combined osteogenesis imperfecta and Ehlers-Danlos syndrome, J. Bone Miner. Res. 29 (6) (2014) 1412–1423.
[21] D.W. Dempster, J.E. Compston, M.K. Drezner, F.H. Glorieux, J.A. Kanis, H. Malluche, P.J. Meunier, S.M. Ott, R.R. Recker, A.M. Parfitt, Standardized nomenclature, symbols, and units for bone histomorphometry: a 2012 update of the report of the ASBMR Histomorphometry Nomenclature Committee, J. Bone Miner. Res. 28 (1) (2013) 2–17.
[22] C.T. Rueden, J. Schindelin, M.C. Hiner, B.E. DeZonia, A.E. Walter, E.T. Arena, K.W. Eliceiri, ImageJ2: ImageJ for the next generation of scientific image data, BMC Bioinformatics 18 (1) (2017) 529.
[23] M.M. Matzuk, M.J. Finegold, J.P. Mather, L. Krummen, H. Lu, A. Bradley, Development of cancer cachexia-like syndrome and adrenal tumors in inhibin-deficient mice, Proc. Natl. Acad. Sci. U. S. A. 91 (19) (1994) 8817–8821.
[24] N. Bechir, E. Pecchi, C. Vilmen, Y. Le Fur, H. Amthor, M. Bernard, D. Bendahan, B. Giannesini, ActRIIB blockade increases force-generating capacity and preserves energy supply in exercising mdx mouse muscle in vivo, FASEB J. 30 (10) (2016) 3551–3562.
[25] C.S. Chiu, N. Peekhaus, H. Weber, S. Adamski, E.M. Murray, H.Z. Zhang, J.Z. Zhao, R. Ernst, J. Lineberger, L. Huang, R. Hampton, B.A. Arnold, S. Vitelli, L. Hamuro, W.R. Wang, N. Wei, G.M. Dillon, J. Miao, S.E. Alves, H. Glantschnig, F. Wang, H.A. Wilkinson, Increased muscle force production and bone mineral density in ActRIIB-Fc-treated mature rodents, J. Gerontol. A Biol. Sci. Med. Sci. 68 (10) (2013) 1181–1192.
[26] E. Ferraro, A.M. Giammarioli, S. Chiandotto, I. Spoletini, G. Rosano, Exercise-induced skeletal muscle remodeling and metabolic adaptation: redox signaling and role of autophagy, Antioxid. Redox Signal. 21 (1) (2014) 154–176.
[27] R. Silbermann, M. Bolzoni, P. Storti, D. Guasco, S. Bonomini, D. Zhou, J. Wu, J.L. Anderson, J.J. Windle, F. Aversa, G.D. Roodman, N. Giuliani, Bone marrow monocyte-/macrophage-derived activin A mediates the osteoclastogenic effect of IL-3 in multiple myeloma, Leukemia 28 (4) (2014) 951–954.
[28] R. Sakai, Y. Eto, M. Ohtsuka, M. Hirafuji, H. Shinoda, Activin enhances osteoclast-like cell formation in vitro, Biochem. Biophys. Res. Commun. 195 (1) (1993) 39–46.
[29] K. Fuller, K.E. Bayley, T.J. Chambers, Activin A is an essential cofactor for osteoclast induction, Biochem. Biophys. Res. Commun. 268 (1) (2000) 2–7.
[30] D. Gaddy-Kurten, J.K. Coker, E. Abe, R.L. Jilka, S.C. Manolagas, Inhibin suppresses and activin stimulates osteoblastogenesis and osteoclastogenesis in murine bone marrow cultures, Endocrinology 143 (1) (2002) 74–83.
[31] T.W. Fowler, A. Kamalakar, N.S. Akel, R.C. Kurten, L.J. Suva, D. Gaddy, Activin A inhibits RANKL-mediated osteoclast formation, movement and function in murine bone marrow macrophage cultures, J. Cell Sci. 128 (4) (2015) 683–694.
[32] K.E. O'Connell, W. Guo, C. Serra, M. Beck, L. Wachtman, A. Hoggatt, D. Xia, C. Pearson, H. Knight, M. O'Connell, A.D. Miller, S.V. Westmoreland, S. Bhasin, The effects of an ActRIIb receptor Fc fusion protein ligand trap in juvenile simian immunodeficiency virus-infected rhesus macaques, FASEB J. 29 (4) (2015) 1165–1175.
[33] O. Hashimoto, M. Funaba, Activin in glucose metabolism, Vitam. Horm. 85 (2011) 217–234.
[34] H. Wu, K. Mezghenna, P. Marmol, T. Guo, A. Moliner, S.N. Yang, P.O. Berggren, C.F. Ibanez, Differential regulation of mouse pancreatic islet insulin secretion and Smad proteins by activin ligands, Diabetologia 57 (1) (2014) 148–156.
[35] R. Pearsall, D. Sako, J. Liu, M. Davies, K. Heveron, R. Castonguay, L. Krishnan, M. Troy, K. Liharska, R. Steeves, M. Cannell, M. Alimzhanov, A. Grinberg, R. Kumar, G.P.107 - ACE-2494, a novel GDF ligand trap, increases muscle and bone mass upon systemic administration in mice, Neuromuscul. Disord. 25 (Supplement 2) (2015) S218.
[36] B.C. Goh, V. Singhal, A.J. Herrera, R.E. Tomlinson, S. Kim, M.C. Faugere, E.L. Germain-Lee, T.L. Clemens, S.J. Lee, D.J. DiGirolamo, Activin receptor type 2A (ACVR2A) functions directly in osteoblasts as a negative regulator of bone mass, J. Biol. Chem. 292 (33) (2017) 13809–13822.
[37] T. Ikenoue, S. Jingushi, K. Urabe, K. Okazaki, Y. Iwamoto, Inhibitory effects of activin-a on osteoblast differentiation during cultures of fetal rat calvarial cells, J. Cell. Biochem. 75 (2) (1999) 206–214.
[38] Y. Qin, Y. Peng, W. Zhao, J. Pan, H. Ksiezak-Reding, C. Cardozo, Y. Wu, P. Divieti Pajevic, L.F. Bonewald, W.A. Bauman, W. Qin, Myostatin inhibits osteoblastic differentiation by suppressing osteocyte-derived exosomal microRNA-218: a novel mechanism in muscle-bone communication, J. Biol. Chem. 292 (26) (2017) 11021–11033.
[39] M. Baroncelli, K. Drabek, M. Eijken, J. van de Peppel, J. Van Leeuwen, A single 2-day pulse of activin-A leads to a transient change in gene expression eventually followed by reduction in extracellular matrix mineralization, Annual European Calcified Tissue Society Congress, Bone Abstracts by Bioscientifica, Rome, Italy, 2016, p. P158.
[40] M. Funaba, K. Ogawa, M. Abe, Expression and localization of activin receptors during endochondral bone development, Eur. J. Endocrinol. 144 (1) (2001) 63–71.
[41] S. Mitsugi, W. Ariyoshi, T. Okinaga, T. Kaneuji, Y. Kataoka, T. Takahashi, T. Nishihara, Mechanisms involved in inhibition of chondrogenesis by activin-A, Biochem. Biophys. Res. Commun. 420 (2) (2012) 380–384.
[42] M. Elkasrawy, S. Fulzele, M. Bowser, K. Wenger, M. Hamrick, Myostatin (GDF-8) inhibits chondrogenesis and chondrocyte proliferation in vitro by suppressing Sox-9 expression, Growth Factors 29 (6) (2011) 253–262.
[43] F. Djouad, W.M. Jackson, B.E. Bobick, S. Janjanin, Y. Song, G.T. Huang, R.S. Tuan, Activin A expression regulates multipotency of mesenchymal progenitor cells, Stem Cell Res Ther 1 (2) (2010) 11.
[44] R.S. Struthers, D. Gaddy-Kurten, W.W. Vale, Activin inhibits binding of transcription factor Pit-1 to the growth hormone promoter, Proc. Natl. Acad. Sci. U. S. A. 89 (23) (1992) 11451–11455.
[45] L.M. Bilezikjian, N.J. Justice, A.N. Blackler, E. Wiater, W.W. Vale, Cell-type specific modulation of pituitary cells by activin, inhibin and follistatin, Mol. Cell. Endocrinol. 359 (1–2) (2012) 43–52.
[46] N.A. Cataldo, V.Y. Fujimoto, R.B. Jaffe, Interferon-gamma and activin A promote insulin-like growth factor-binding protein-2 and -4 accumulation by human luteinizing granulosa cells, and interferon-gamma promotes their apoptosis, J. Clin. Endocrinol. Metab. 83 (1) (1998) 179–186.
[47] T. Puolakkainen, P. Rummukainen, J. Lehto, O. Ritvos, A. Hiltunen, A.M. Saamanen, R. Kiviranta, Soluble activin type IIB receptor improves fracture healing in a closed tibial fracture mouse model, PLoS One 12 (7) (2017) e0180593.
[48] T.A. Souza, X. Chen, Y. Guo, P. Sava, J. Zhang, J.J. Hill, P.J. Yaworsky, Y. Qiu, Proteomic identification and functional validation of activins and bone morphogenetic protein 11 as candidate novel muscle mass regulators, Mol. Endocrinol. 22 (12) (2008) 2689–2702.
[49] K.M. Attie, N.G. Borgstein, Y. Yang, C.H. Condon, D.M. Wilson, A.E. Pearsall, R. Kumar, D.A. Willins, J.S. Seehra, M.L. Sherman, A single ascending-dose study of muscle regulator ACE-031 in healthy volunteers, Muscle Nerve 47 (3) (2013) 416–423.
[50] C. Campbell, H.J. McMillan, J.K. Mah, M. Tarnopolsky, K. Selby, T. McClure, D.M. Wilson, M.L. Sherman, D. Escolar, K.M. Attie, Myostatin inhibitor ACE-031 treatment of ambulatory boys with Duchenne muscular dystrophy: results of a randomized, placebo-controlled clinical trial, Muscle Nerve 55 (4) (2017) 458–464.
[51] S.J. Lee, L.A. Reed, M.V. Davies, S. Girgenrath, M.E. Goad, K.N. Tomkinson, J.F. Wright, C. Barker, G. Ehrmantraut, J. Holmstrom, B. Trowell, B. Gertz, M.S. Jiang, S.M. Sebald, M. Matzuk, E. Li, L.F. Liang, E. Quattlebaum, R.L. Stotish, N.M. Wolfman, Regulation of muscle growth by multiple ligands signaling through activin type II receptors, Proc. Natl. Acad. Sci. U. S. A. 102 (50) (2005) 18117–18122.
[52] B.M. Morrison, J.L. Lachey, L.C. Warsing, B.L. Ting, A.E. Pullen, K.W. Underwood, R. Kumar, D. Sako, A. Grinberg, V. Wong, E. Colantuoni, J.S. Seehra, K.R. Wagner, A soluble activin type IIB receptor improves function in a mouse model of amyotrophic lateral sclerosis, Exp. Neurol. 217 (2) (2009) 258–268.